ELSEVIER

Journal of Alloys and Compounds 464 (2008) 446–451

Journal of ALLOYS AND COMPOUNDS

www.elsevier.com/locate/jallcom

Electrical discharge machining of a NiAlFe ternary shape memory alloy

S.L. Chen [a,*], S.F. Hsieh [b], H.C. Lin [c], M.H. Lin [a], J.S. Huang [b]

[a] *Department of Mechanical Engineering, National Kaohsiung University of Applied Sciences, Kaohsiung 807, Taiwan, ROC*
[b] *Department of Mold and Die Engineering, National Kaohsiung University of Applied Sciences, Kaohsiung 807, Taiwan, ROC*
[c] *Department of Materials Science and Engineering, National Taiwan University, Taipei 106, Taiwan, ROC*

Received 15 August 2007; received in revised form 30 September 2007; accepted 2 October 2007
Available online 7 October 2007

Abstract

The electro-discharge machining (EDM) characteristics of a NiAlFe ternary shape memory alloy (SMA) have been investigated in this study. Experimental results reveal that the material removal rates (MRRs) of $Ni_{60}Al_{24.5}Fe_{15.5}$ and $Ti_{35.5}Ni_{49.5}Zr_{15}$ alloys in the EDM process exhibit a reverse relationship to the product of the alloy's melting temperature and thermal conductivity. In addition, a precise EDM machining of NiAlFe SMA can be obtained by setting the machine parameters at low pulse energy. The surface roughness (Ra) of the EDMed NiAlFe SMA is found to follow the empirical equation of $Ra = \lambda(I_P \times \tau_P)^{\beta}$. Having a less $T_\Theta \times K_T$ value, $Ni_{60}Al_{24.5}Fe_{15.5}$ alloy has a larger Ra value than that of $Ti_{35.5}Ni_{49.5}Zr_{15}$ alloy after electro-discharge machining. The recast layer consists of the oxides Fe_2O_3, Al_2O_3, NiO and the deposition particles of the consumed Cu electrode and dissolved dielectric medium. The hardening effect near the outer surface for EDMed NiAlFe alloy originates from the recast layer. The thickness of the recast layer varies with the pulse duration and exhibits a minimum value at the maximal MRR.
© 2007 Elsevier B.V. All rights reserved.

Keywords: EDM; Roughness; NiAlFe shape memory alloys

1. Introduction

Among many shape memory alloys (SMAs), TiNi alloys are the most popular due to their superior properties in shape memory effect (SME) and superelasticity [1–4]. However, the applications of these alloys are limited to use at temperatures lower than 100 °C. For this reason, high-temperature SMAs need to be developed and studied. Nickel-rich NiAl alloys containing about 63–65 at.% Ni have been reported as promising shape memory alloys. The quenched Nickel-rich NiAl alloys undergo a thermoelastic martensitic transformation from a B2 (β-phase) structure to a metastable $L1_0$ structure with either 3R or 7R stacking. The martensitic transformation starting temperature Ms of the β-phase occurs over a wide temperature range up to approximately 500 °C, depending on the nickel content [5,6]. However, only a small bending shape memory effect was found due to its limited ductility [7–9]. Adding Fe to NiAl binary SMAs is used for ductility and SME improvement [10–15]. Some authors used rapid solidification to produce a ductile NiAlFe alloy with the quench-induced martensite structure that exhibited a reversible SME [13,16]. Ishida et al. also found that with proper heat treatments and quenching procedures, the cast material could be produced with room temperature ductility and shape recovery [15,17].

Ni–Al binary system has drawn much attention for many years owing to their importance in the development of high-temperature materials, i.e. it shows excellent oxidation resistance and has the advantageous of heat conductivity [7,18], as well as high SMAs [5–6]. Unfortunately, they are difficult for machine and hot working due to ordered structure. To overcome machining difficulty in the manufacturing process, some special techniques, such as the electrical discharge machining (EDM) and laser machining, may be useful in machining the hard, brittle and tough materials [19–21]. The die-sinking EDM process is a non-traditional, thermoelectric process in which the material is removed by electro-discharges occurring between the workpiece and tool electrode immersed in a liquid dielectric medium. The electrical discharge melts and vaporizes minute amounts of the workpiece, which are then ejected and swept away by the dielectric. Hence, EDM is an effective technique in machining the difficult-to-cut materials. To extend the applications of NiAlFe ternary SMAs, some machining technologies for the production

* Corresponding author. Tel.: +886 7 381 4526x5342; fax: +886 7 383 5015.
E-mail address: slchen@cc.kuas.edu.tw (S.L. Chen).

0925-8388/$ – see front matter © 2007 Elsevier B.V. All rights reserved.
doi:10.1016/j.jallcom.2007.10.012

Table 1
The machining parameters of EDM in this study

Discharge current (A)	3, 6, 10, 19
Pulse duration (μs)	3, 6, 12, 25, 50, 100
Pause duration (μs)	3, 6, 12, 25, 50, 100
Gap voltage (V)	50
Electrode	Cu (+); workpiece (−)
Dielectric	Kerosene

of complicated shapes with high accuracy should be urgently developed. Therefore, the objective of this study is to investigate the machining characteristics of NiAlFe alloys involving EDM. The microstructure, composition, roughness and hardness of EDMed surfaces are discussed. The $Ti_{35.5}Ni_{49.5}Zr_{15}$ high-temperature SMA is used as a comparative material.

2. Experimental procedure

The conventional tungsten arc-melting technique was employed to prepare the $Ni_{60}Al_{24.5}Fe_{15.5}$ ternary alloy. Nickel (purity, 99.9 wt.%), Aluminum (purity, 99.9 wt.%), and iron (purity, 99.95 wt.%), totaling about 180 g, were melted and remelted at least six times in an argon atmosphere. Pure titanium buttons were also melted and used as getters. The mass loss during melting was negligibly small. The as-melted buttons were homogenized at 1200 °C for 72 h. The homogenized buttons were cut into several plates with a low speed diamond saw. Specimens for the electro-discharge machining (size: 55 mm × 20 mm × 5 mm) were carefully cut and ground from these plates. The specimens were then evacuated in quartz tubes and annealed at 1150 °C for 2 h, followed by a water-quench.

The EDM specimens were performed on a die-sinking EDM machine model type 30-TP, made by Topedm Co. in Taiwan. The operation parameters used in this study are presented in Table 1. The microstructures of electro-discharge machined (EDMed) surfaces were examined using X-ray diffraction (XRD), scanning electron microscopy (SEM) and secondary electron image (SEI). The X-ray analyses of EDMed surfaces were performed at room temperature by a Siemens D5000 XRD using Cu Kα radiation. The power was 30 kV × 20 mA and the 2θ scanning rate was 3 min^{-1}. The morphologies of EDMed surface were observed using a JOEL 6330 TF SEM with SEI facility. A Talysurf profilometer was used to evaluate quantitatively the roughness of the EDMed surface, presented by Ra. The cut-off is selected as 0.8 mm. For each piece, the average of readings taken at seven places on machining plane was chosen as the surface roughness value. The surface hardness was measured in a microvickers hardness tester with a load of 25 g for 15 s. For each specimen, the average hardness value was taken from at least five test readings.

3. Results and discussion

3.1. The material removal rate and surface roughness of a NiAlFe alloy after EDM process

Table 2 presents the transformation temperatures, hardness and crystal structures at room temperature for $Ni_{60}Al_{24.5}Fe_{15.5}$ and $Ti_{35.5}Ni_{49.5}Zr_{15}$ ternary SMAs. Some important metallurgical properties of NiAlFe alloy in Table 2 aid to investigate the machining characteristics of this alloy in the EDM process. From this Table, one can find that $Ni_{60}Al_{24.5}Fe_{15.5}$ and $Ti_{35.5}Ni_{49.5}Zr_{15}$ alloys exhibit the mixture of β′ martensite and γ-phase, and $(Ti,Zr)_2Ni$, λ_1-phase and B19′ phase, respectively. The material's intrinsic properties and several machining parameters, e.g. the electrode material, electrode polarity, discharge current I_P and pulse duration τ_P, can significantly affect the EDM characteristics.

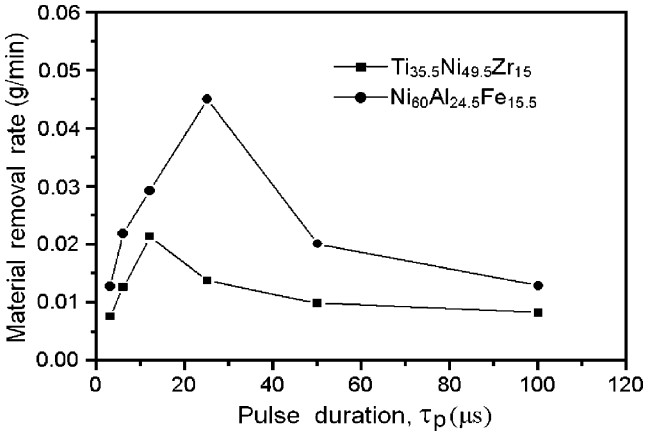

Fig. 1. The material removal rate vs. the pulse duration τ_P at $I_P = 10$ A for the $Ni_{60}Al_{24.5}Fe_{15.5}$ and $Ti_{35.5}Ni_{49.5}Zr_{15}$ alloys.

In this study, we hope to determine the effect of some of the most important parameters implicated in the EDM process on a NiAlFe ternary alloy including discharge current I_P and pulse duration τ_P. Fig. 1 depicts the material removal rate (MRR) versus the pulse duration at $I_P = 10$ A for $Ni_{60}Al_{24.5}Fe_{15.5}$ and $Ti_{35.5}Ni_{49.5}Zr_{15}$ alloys. As can be seen from Fig. 1, the MRR of $Ni_{60}Al_{24.5}Fe_{15.5}$ alloy is larger than that of $Ti_{35.5}Ni_{49.5}Zr_{15}$ alloy [22] at various pulse durations during the EDM process. This feature is associated with their melting temperature (T_Θ) and thermal conductivity (K_T). Materials with higher melting temperature, leading to less melting and evaporation, and higher thermal conductivity, causing more heat transfer of discharge energy to the nearby matrix, will show a lower MRR in the EDM process. Hence, the product of the melting temperature and thermal conductivity of materials can be used to evaluate the EDM characteristic in NiAlFe and TiNiZr ternary SMAs. The MRRs of TiNi-based SMAs have a reverse relationship to the product of the materials' melting temperature and thermal conductivity [20,22]. Table 3 presents the product of the melting temperature and thermal conductivity of $Ni_{60}Al_{24.5}Fe_{15.5}$ and $Ti_{35.5}Ni_{49.5}Zr_{15}$ alloys. A careful examination of Fig. 1 and Table 3 shows that the MRRs of $Ni_{60}Al_{24.5}Fe_{15.5}$ and $Ti_{35.5}Ni_{49.5}Zr_{15}$ alloys are in accordance with the above-mentioned relationship.

Table 2
The crystal structures and some basic properties of $Ni_{60}Al_{24.5}Fe_{15.5}$ and $Ti_{35.5}Ni_{49.5}Zr_{15}$ ternary alloys

Alloy	M* (°C)	A* (°C)	Hardness (Hv)	Crystal structure
$Ni_{60}Al_{24.5}Fe_{15.5}$	171 (B2 → β′)	205 (β′ → B2)	260	β′ + γ-phase
$Ti_{35.5}Ni_{49.5}Zr_{15}$	176	217	320	B19′ + λ_1-phase + $(Ti,Zr)_2Ni$

M*, A*: DSC peak temperatures of forward and reverse martensitic transformations, respectively.

Table 3
The product of the melting temperature and thermal conductivity of $Ni_{60}Al_{24.5}Fe_{15.5}$ and $Ti_{35.5}Ni_{49.5}Zr_{15}$ ternary alloys

Alloy	$T_\Theta \times K_T$ (W/cm °C)
$Ni_{60}Al_{24.5}Fe_{15.5}$	292.0
$Ti_{35.5}Ni_{49.5}Zr_{15}$	470.4

Fig. 2 shows the relationship between the MRR and the pulse duration at various discharge currents for the $Ni_{60}Al_{24.5}Fe_{15.5}$ alloy. It can be seen that the MRR increases upon increasing the discharge current. Similar characteristics can be also found when electro-discharge machining of Cu–Be alloys [23]. A high-discharge current can have a high-current density [24]. This feature will obviously promote the material's melting and evaporation and the impact force of expanded dielectric medium. Hence, a higher MRR occurs at a higher discharge current during the EDM process. Besides, one can also find in Figs. 1 and 2 that the MRRs initially increase with the pulse duration, reach maximum values, and then decrease to constant values for various discharge currents. The MRR is also expected to increase with pulse duration, because its high-accumulated electro-discharge energy will rapidly melt and evaporate the material. Moreover, an extended pulse duration will expand the plasma channel [25]. The EDM covered area is widened and the average energy density is decreased, leading to a decrease in MRR. From these results, it is clear that the MRR cannot be enhanced simply by lengthening the pulse duration. In other words, it is necessary to consider the discharge current I_P and pulse duration τ_P parameters in combination. Therefore, there appears an optimal pulse duration, $\tau_P = 12–25$ μs in Fig. 1, to have a maximum MRR.

As well as the workpiece, the Cu electrode will also slightly melt and evaporate during EDM. To possess the high accuracy and efficiency of EDM, it is important to understand the consumption of electrode material. Fig. 3 reveals the electrode wear rate (EWR) versus the pulse duration at various discharge currents for the $Ni_{60}Al_{24.5}Fe_{15.5}$ alloy. It indicates that the EWR initially increases, reaches a maximum value and then decreases with growing pulse duration. This variation of the EWR with pulse duration depicts a similar tendency to that of the MRR

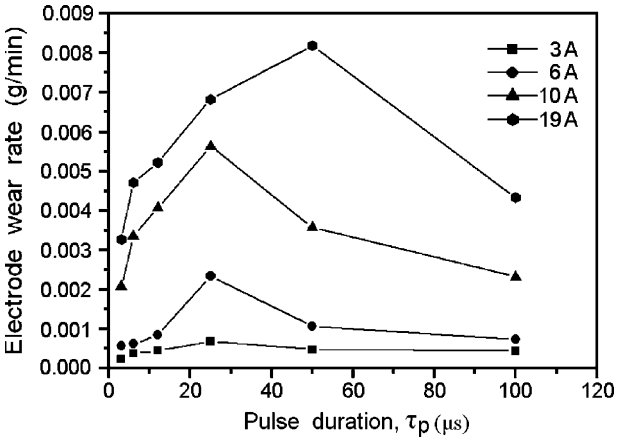

Fig. 3. The electrode wear rate vs. the pulse duration τ_P at various discharge currents I_P for the $Ni_{60}Al_{24.5}Fe_{15.5}$ alloy.

with pulse duration shown in Fig. 2. The electro-discharge energy mode also has a significant effect on the EWR. The similar variations of the MRR and EWR with discharge current and pulse duration shown in Figs. 2 and 3 also occurs when electro-discharge machining $Ti_{35.5}Ni_{49.5}Zr_{15}$ alloy. These features reveal that the $Ni_{60}Al_{24.5}Fe_{15.5}$ and $Ti_{35.5}Ni_{49.5}Zr_{15}$ alloys show similar EDM characteristics although they have different crystal structures and mechanical properties at room temperature.

Fig. 4 shows the roughness of EDMed surface versus the pulse duration τ_P at various discharge currents I_P for the $Ni_{60}Al_{24.5}Fe_{15.5}$ alloy. The surface roughness on the machined surface varies from 1.5 to 3.8 μm. This result indicates that the increased discharge current and pulse duration can increase the roughness of EDMed surface. High-discharge current affords the large amount of discharges to strike the workpiece surface more intensely, and the resulting worsened erosion effect brings about a deterioration of the surface roughness. Furthermore, the longer pulse duration gives greater discharge energy to melt and penetrate deeper into the material, which generates larger and deeper discharge craters, leading to an increased surface roughness on the workpiece [25]. Based on the above discussion, an excellent machined surface finish on NiAlFe SMA can be obtained by

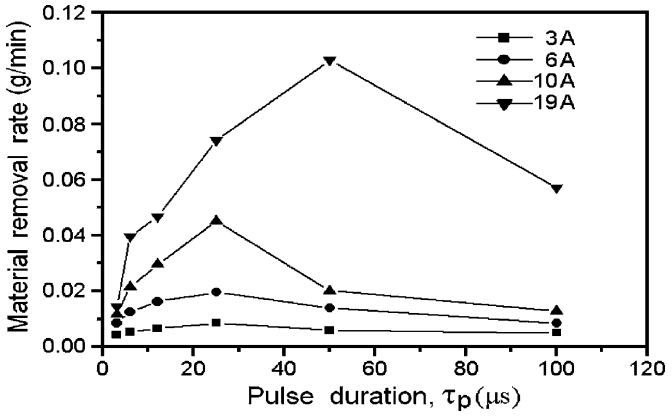

Fig. 2. Relationship between the MRR and EDM parameters for the $Ni_{60}Al_{24.5}Fe_{15.5}$ alloy.

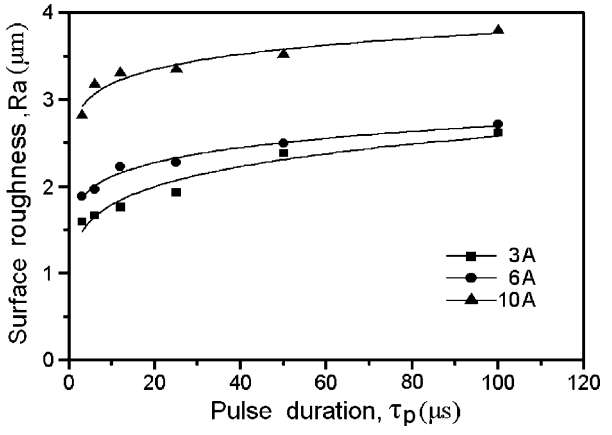

Fig. 4. The surface roughness vs. the pulse duration τ_P at various discharge currents I_P for the $Ni_{60}Al_{24.5}Fe_{15.5}$ alloy.

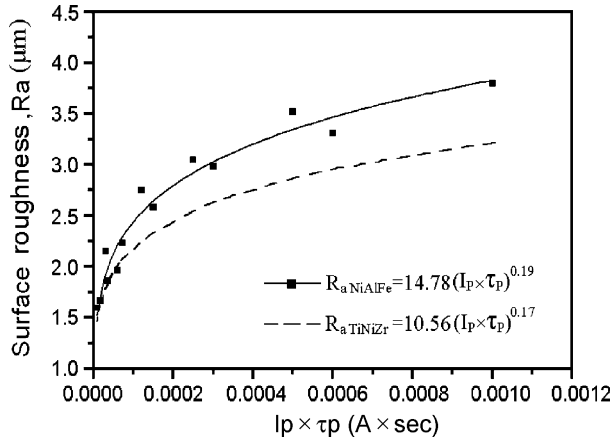

Fig. 5. The surface roughness vs. the product of I_P and τ_P for the EDMed $Ni_{60}Al_{24.5}Fe_{15.5}$ and $Ti_{35.5}Ni_{49.5}Zr_{15}$ alloys [22].

setting the machine parameters at a lower discharge current I_P and a shorter pulse duration τ_P, but this approach takes more time.

Fig. 5 depicts the surface roughness Ra versus the product of the discharge current I_P and pulse duration τ_P for the $Ni_{60}Al_{24.5}Fe_{15.5}$ alloy. A comparison of roughness Ra values obtained for the $Ti_{35.5}Ni_{49.5}Zr_{15}$ alloy [22] is also shown in Fig. 5. The roughness of an EDMed surface increases with growing pulse energy and can be represented by an empirical equation of $Ra = \lambda(I_P \times \tau_P)^{\beta}$, where the constants λ and β depend on the tool-work material combination, including the work material's structures, thermal properties, mechanical properties, electrode materials and the electro-discharge energy mode [23,26]. From the curves shown in Fig. 5, the roughness of the EDMed surface is found to follow the equation $Ra = 14.78(I_P \times \tau_P)^{0.19}$ for $Ni_{60}Al_{24.5}Fe_{15.5}$ alloy, but $Ra = 10.56(I_P \times \tau_P)^{0.17}$ for $Ti_{35.5}Ni_{49.5}Zr_{15}$ alloy. The values of the constants λ and β were determined by fitting the curve by the least-squares method. The Ra value of the $Ni_{60}Al_{24.5}Fe_{15.5}$ alloy after electro-discharge machining is larger than that of $Ti_{35.5}Ni_{49.5}Zr_{15}$ alloy, as shown in Fig. 5. We propose that the Ra value is also related to the materials' thermal conductivity and melting temperature in ternary SMAs. The greater the MRR and Ra value is, the less the $T_\Theta \times K_T$ value will be. In other words, the roughness of the EDMed surface is smaller for the alloy having a higher $T_\Theta \times K_T$ value. The same characteristics also occurs when electro-discharge machining $Ti_{50}Ni_{50}$ and $Ti_{49}Ni_{51}$ binary alloys [20].

3.2. Surface morphology and composition analysis of a NiAlFe SMA after EDM process

EDM sparks erode the surfaces randomly. Fig. 6 reveals that the surface morphology of the $Ni_{60}Al_{24.5}Fe_{15.5}$ ternary SMA after EDM process. It is characterized by melting drops, discharge craters and recast materials. Fig. 7 shows the XRD patterns of the EDMed surface layer for the $Ni_{60}Al_{24.5}Fe_{15.5}$ alloy. It indicates that the XRD peaks of Fe_2O_3, Al_2O_3, NiO, Ni_3Al, C and Cu_2O are observed. The formation of Fe_2O_3, Al_2O_3 and NiO

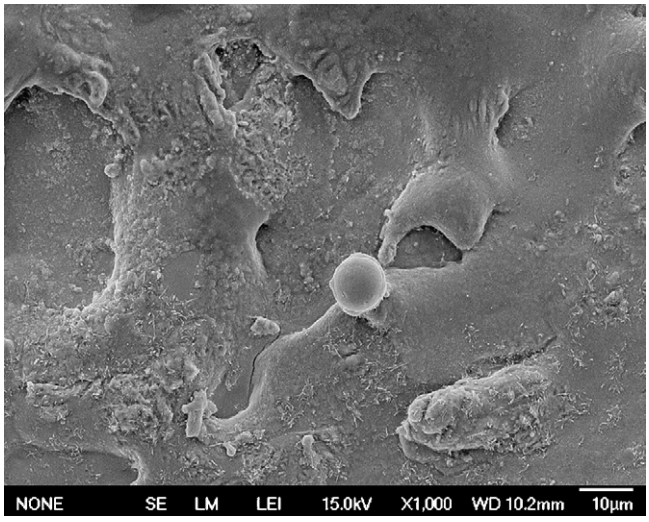

Fig. 6. The SEM micrograph of the EDMed surface for the $Ni_{60}Al_{24.5}Fe_{15.5}$ alloy.

oxides is ascribed to the high activity of Fe, Al and Ni atoms. The presence of Cu_2O and C is due to the deposition of the consumed Cu electrode and kerosene dielectric medium. Fig. 8 reveals the specimen's hardness at various distances form the EDMed surface of the $Ni_{60}Al_{24.5}Fe_{15.5}$ alloy under the conditions of $I_P = 10$ A and $\tau_P = 100$ μs. It indicates that the specimen's hardness near the outer surface can reach 527 Hv. This hardening effect arises from the formation of the oxides Fe_2O_3, Al_2O_3, NiO and the deposition particles in the recast layer. In addition, the hardness of matrix in $Ni_{60}Al_{24.5}Fe_{15.5}$ alloy is not affected by the EDM process.

As mentioned above, lots of recast materials deposit on the EDMed surface of the NiAlFe alloys. Fig. 9a–d present the cross-sectional SEI micrographs near the EDMed surface layer for the $Ni_{60}Al_{24.5}Fe_{15.5}$ alloy under the conditions of $I_P = 10$ A and $\tau_P = 6$, 12, 25, 100 μs, respectively. Carefully examining Fig. 9a–d, the thickness of the recast layer varies with the pulse duration. It indicates that the thickness of the recast layer initially increases with growing pulse duration up to $\tau_P = 12$ μs,

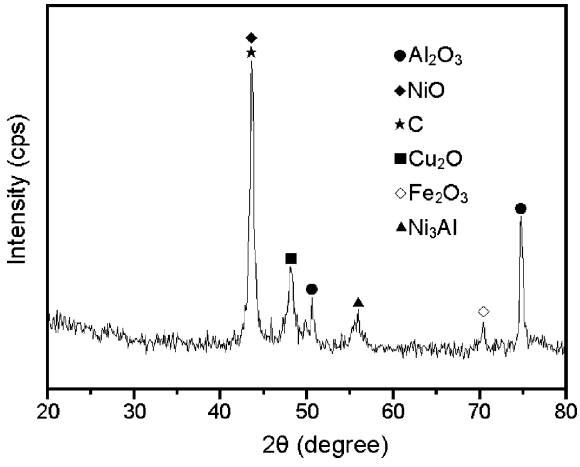

Fig. 7. The XRD patterns of the EDMed surface layer for the $Ni_{60}Al_{24.5}Fe_{15.5}$ alloy.

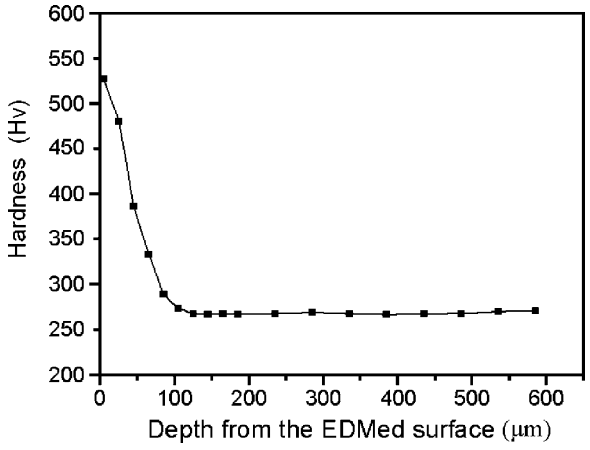

Fig. 8. The specimen's hardness at various distance from the EDMed surface of $Ni_{60}Al_{24.5}Fe_{15.5}$ alloy under the condition $I_P = 10$ A and $\tau_P = 100$ μs.

and drops to a minimum value as well as a maximum MRR at $\tau_P = 25$ μs, and then the thickness increases again in the over-long pulse duration ($\tau_P = 100$ μs). This is explained in the following. During the EDM process, the electrode-discharge plasma channel is composed of ion and electron flows. Electron flow is dominant in the plasma channel in the initial stage, and hence the cathode (workpiece) has lower electro-discharge energy. Meanwhile, the ratio of positive ions flow in the plasma channel increases with growing pulse duration [24] and the workpiece has greater discharge energy, and hence the thickness of the recast layer grows in the beginning pulse duration ($\leq$12 μs). Thereafter, for the optimal pulse duration at the maximal MRR, the high-electro-discharge energy provides the dielectric medium to have violent impact force to effectively expel the molten materials and the deposited particles from the EDMed surface, and hence the recast layer becomes thinner, as shown in Fig. 9c. An over-long pulse duration will have relatively high-accumulated electro-discharge energy. This makes more material be melted and re-solidified, as well as more kerosene dielectric medium be dissolved and deposited on the EDMed surface. If this molten material is not flushed away from the surface by the dielectric, it will solidify during the cooling process and form a recast layer. Hence, the thickness of the recast layer is increased again.

4. Conclusion

The EDM characteristics of a NiAlFe ternary shape memory alloy have been investigated in this study. The important conclusions are as follows:

(1) The MRR of a $Ni_{60}Al_{24.5}Fe_{15.5}$ ternary SMA in the EDM process significantly relates to the electro-discharge energy mode. It increases monotonically with growing discharge current, but appears at the optimal pulse duration, $\tau_P = 25$ μs at $I_P = 10$ A in this study, to have a maximum value. In addition, the MRRs of $Ni_{60}Al_{24.5}Fe_{15.5}$ and $Ti_{35.5}Ni_{49.5}Zr_{15}$ ternary SMAs are found to have a reverse relationship to the product of the material's melting temperature and thermal conductivity. Meanwhile, a lower discharge current I_P and

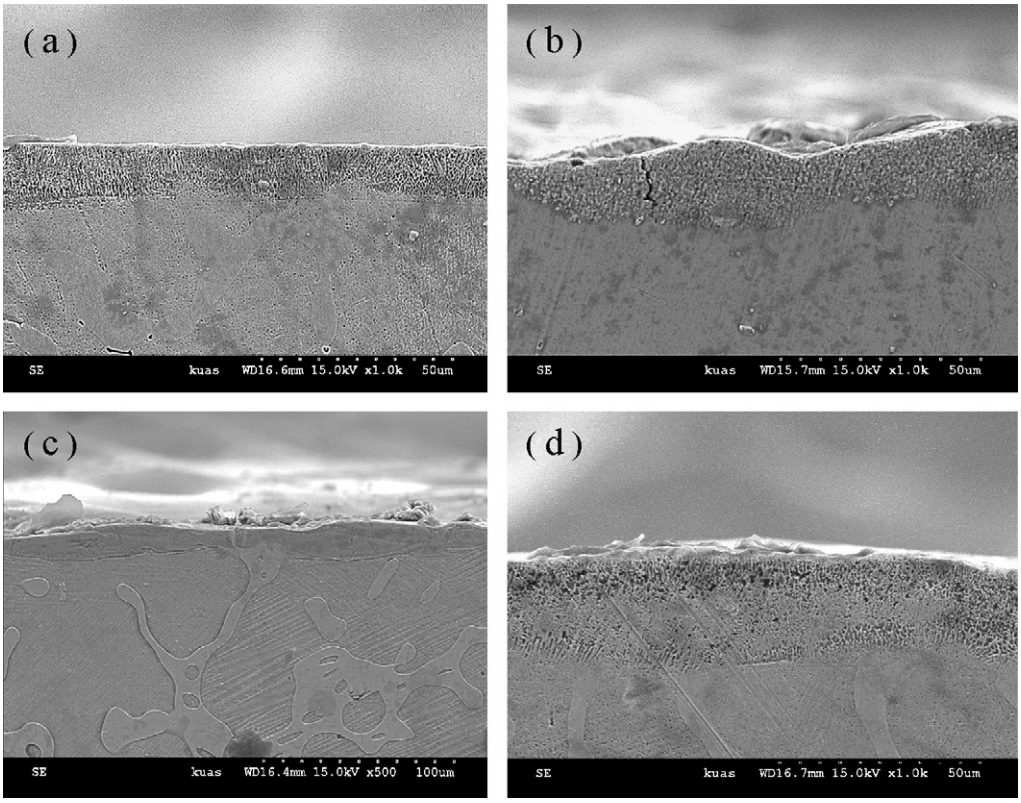

Fig. 9. The cross-sectional SEI micrographs near the EDMed surface layer for the $Ni_{60}Al_{24.5}Fe_{15.5}$ alloy under the conditions of $I_P = 10$ A and τ_P (a) 6 μs, (b) 12 μs, (c) 25 μs, and (d) 100 μs.

a shorter pulse duration τ_P should be selected to have an excellent machined surface finish on a NiAlFe alloy.

(2) The EDMed $Ni_{60}Al_{24.5}Fe_{15.5}$ ternary SMAs demonstrate increasing surface roughness as the discharge current and pulse duration increase. The roughness of EDMed surface increases with the discharge current and pulse duration, and follows the empirical equation $Ra = \lambda(I_P \times \tau_P)^{\beta}$. The $Ni_{60}Al_{24.5}Fe_{15.5}$ alloy, having a less $T_\Theta \times K_T$ value, exhibits a rougher EDMed surface than that of $Ti_{35.5}Ni_{49.5}Zr_{15}$ alloy.

(3) The thickness of the recast layer increases in the early stage, drops to the minimum value at the maximal MRR, and then grows in the extended pulse duration again. The recast layer consists of the oxides Fe_2O_3, Al_2O_3, NiO and the deposition particles of the consumed Cu electrode and dissolved dielectric medium in the recast layer.

(4) The specimen's hardness near the outer surface can reach 527 Hv for EDMed $Ni_{60}Al_{24.5}Fe_{15.5}$ alloy, but, the hardness of the matrix is not affected by the EDM process. This hardening effect is due to the formation of the oxides Fe_2O_3, Al_2O_3, NiO and the deposition particles of the consumed Cu electrode and dissolved dielectric medium in the recast layer.

Acknowledgements

The authors sincerely acknowledge the financial support of this research by the National Science Council (NSC), Republic of China, under the grant NSC 95-2221-E-151-013.

References

[1] S. Miyazaki, K. Otsuka, ISIJ Int. 29 (1989) 353–377.
[2] K. Gall, H.J. Maier, Acta Mater. 50 (2002) 4643–4657.
[3] S. Miyazaki, T. Imai, Y. Igo, K. Otsuka, Metall. Trans. 17A (1986) 115–120.
[4] Y. Liu, I. Houver, H. Xiang, L. Bataillard, S. Miyazaki, Metall. Trans. 30A (1981) 1275–1282.
[5] Y.K. Au, C.M. Wayman, Scipta Metall. 6 (1972) 1209–1214.
[6] J.H. Yang, C.M. Wayman, Intermetallics 2 (1994) 111–119.
[7] U.D. Hangen, G. Sauthoff, Intermetallics 7 (1999) 501–510.
[8] P.L. Potapov, N.A. Poliakova, V.A. Udovenko, Scripta Metall. 35 (1996) 423–427.
[9] Y.D. Kim, C.M. Wayman, Metall. Trans. 23A (1992) 2981–2986.
[10] J.A. Horton, C.T. Liu, E.P. George, Mater. Sci. Eng. 192–193A (1995) 873–880.
[11] C.Y. Xie, J.S. Wu, Intermetallics 8 (2000) 77–80.
[12] C.Y. Xie, L.W. Sen, T.Y. Hsu, Scripta Mater. 35 (1996) 345–348.
[13] S. Furukawa, A. Inoue, T. Masumoto, Mater. Sci. Eng. 98 (1988) 515–518.
[14] J.H. Yang, C.M. Wayman, Mater. Sci. Eng. 160A (1993) 241–249.
[15] R. Kainuma, K. Ishida, T. Nishizawa, Metall. Trans. 23A (1992) 1147–1153.
[16] R. Kainuma, H. Nakano, K. Oikawa, K. Ishida, T. Nishizawa, Mater. Res. Soc. Symp. Proc. 246 (1992) 403–408.
[17] K. Ishida, R. Kainuma, N. Ueno, T. Nishizawa, Metall. Trans. 22A (1991) 441–446.
[18] D.B. Miracle, R. Darolia, in: J.H. Westbrook, R.L. Fleischer (Eds.), Structural Application of Intermetallic Compound, John Wiely & Sons Ltd., Chichester, 2000, p. 55.
[19] S.H. Lee, X. Li, J. Mater. Process. Tech. 139 (2003) 315–321.
[20] H.C. Lin, K.M. Lin, I.S. Cheng, J. Mater. Sci. 36 (2001) 399–404.
[21] S.L. Chen, B.H. Yan, F.Y. Huang, J. Mater. Process. Tech. 87 (1999) 107–111.
[22] S.L. Chen, S.F. Hsieh, H.C. Lin, M.H. Lin, J.S. Huang, Mater. Sci. Eng. 445–446A (2007) 486–492.
[23] J.C. Rebelo, A. Morao Dias, D. Kermer, J.L. Lebrun, J. Mater. Process. Tech. 103 (2000) 389–397.
[24] D.D. Dibitonto, P.T. Eubank, M.R. Patel, J. Appl. Phys. 66 (1989) 4095–4103.
[25] A.M. Gadalla, B. Bozkurt, J. Mater. Res. 7 (1992) 2853–2858.
[26] M.L. Jeswani, Wear 51 (1978) 227–236.